RSC Advances

ROYAL SOCIETY
OF **CHEMISTRY**

www.rsc.org/advances

Greener Saponin Induced Morphologically Controlled Various Polymorphs of Nanostructured Iron oxide Materials for Biosensor Applications

Sasikala Sundar and Shakkthivel Piraman*

Sustainable Energy and Smart Materials Research Lab,
Department of Nanoscience and Technology,
Alagappa University, Karaikudi-630 002,
Tamilnadu, INDIA.

Tel: 04565- 238100, Extn.372
Fax: 04565- 225202, 225525

*Corresponding Author

Email: apsakthivel@yahoo.com

Abstract

Presently, the progress of green chemistry in the synthesis of magnetic nanoparticles with the use of plants has engrossed a great attention, that do not employ toxic chemicals in the synthesis protocols to avoid adverse effects in medical applications. Here, it is a report on rapid, energy-efficient, green and economically scalable room temperature protocol for the synthesis of different polymorphs of iron oxide nanostructures such as Fe_3O_4 nanospheres, γ-Fe_2O_3 nanoribbon and α-Fe_2O_3 nanospheres using greener saponin as a bio-surfactant with tunable magnetic properties directed by particle shape. A bio-surfactant directed growth mechanism was proposed for the magnetic anisotropic structure formation and the aspect ratio can be controlled by changing reaction conditions. The electrochemical sensing properties of the as obtained γ-Fe_2O_3 nanoribbon and α-Fe_2O_3 nanospheres modified glassy carbon electrode (GCE) towards dopamine and uric acid with different morphologies were investigated systematically. The electrochemical dynamic results confirmed that the superior electron transport ability of nanostructures exhibited higher anodic current response with a shift in positive potential than the bare GCE. The γ-Fe_2O_3 nanoribbon showed 100% enhanced electrochemical sensing performance compared to the α-Fe_2O_3 nanospheres. These studies suggested that non-spherical iron oxide nanoparticles (NPs) could potentially lead to further advancement in nanomedicine.

1. Introduction

Acicular iron oxide nanostructures such as needles, nanorods, and nanowires have attracted much attention and research owing to their enhanced mechanical, optical, electrical and electromagnetic properties over spherically shaped nanoparticles.[1-3] Magnetic nanostructures have attracted significant and growing amounts of attention not only because of their fascinating physicochemical properties but also their potential uses in a wide range of applications, including biomedicine, magnetic fluids, magnetic recording, and spin electronics.[4-6] Among the various magnetic materials, the iron oxides (such as hematite, magnetite, and maghemite) represent an important class of magnetic transition metal oxide materials have been widely studied for their excellent physical and chemical properties, but these properties are greatly affected by the synthesis route and nanocrystal's size and shape.[7-10]

The facile synthesis and fabrication of 1D, 2D, and 3D nanoparticle assemblies with highly controlled structures, uniform morphologies, and novel properties is of now emerging as a new field of significance. Techniques that have been used, with varying degree of success, to produce 1D iron oxide nanoparticles include sol-gel method,[11] "wrap_bake_peel" process,[12] temperature-assisted reduction of an akaganeite intermediate,[13] microwave preparation,[14] ultrasound irradiation technique,[15] laser deposition,[16] and electrochemical precipitation methods.[17,18] All of these methods present some draw backs and includes either physical or chemical processes and involves the use of toxic, highly expensive, hazardous, and non-environmentally friendly chemicals. Over the past decade, there has been an increased emphasis on the topic of "green" chemistry and chemical processes. Green synthesis provides an advancement over the chemical and

physical methods as it is cost effective, environment friendly, easily scaled up for large scale synthesis and no need of high pressure, energy, temperature and toxic chemicals.[19]

Herein, we report the green chemistry approach for the synthesis of various polymorphs of iron oxide nanostructures such as Fe_3O_4 nanospheres, γ-Fe_2O_3 nanoribbon and α-Fe_2O_3 nanospheres by simple co-precipitation method through iron ions using Aloe vera (AV) extract as an eco-friendly bio-surfactant containing saponin as a main factor. The effect of reaction time and different concentrations of bio-surfactant on the synthesis of iron oxide superstructures have been investigated. In addition to this, electrocatalytic activity and simultaneous determination of Uric acid (UA) and Dopamine (DA) sensing towards the synthesized materials of γ-Fe_2O_3 nanoribbon and α-Fe_2O_3 nanospheres have been studied. The novelty of the synthesis and different morphological phases of iron oxide nanospheres and nanoribbons are explained with the help of various spectroscopic techniques. To the best of our knowledge, this is the first ever report on facile fabrication of iron oxide nanostructures using AV extract as a bio-surfactant for electrochemical sensing applications.

2. Experimental Section

2.1. Chemicals

Iron (III) chloride hexahydrate ($FeCl_3.6H_2O$), iron (II) sulphate heptahydrate ($FeSO_4.7H_2O$), Sodium hydroxide (NaOH), Uric acid (UA) and Dopamine (DA) were purchased from E-Merck Specialities Products. All chemicals are of reagent grade and were used without further purification. Aloe vera leaves were purchased from the local market. Doubly distilled water was used as the solvent.

2.2. Synthesis of Iron oxide nanostructures

The iron oxide nanostructures were prepared by an aqueous co-precipitation method using $FeCl_3.6H_2O$ and $FeSO_4.7H_2O$. In a typical experimental procedure, 30 ml of $FeCl_3.6H_2O$ solution was mixed with 15 ml of $FeSO_4.7H_2O$ solution in a 3-necked round bottom flask. The prepared saponin rich bio-surfactant (AV extract) was added in to the above mixture and reacted for 1 hr. After that, the NaOH solution was dropped slowly into the solution under vigorous stirring until a pH of 13 was reached and the stirring was continued for another 1 hr. The changes of solution color could be seen from orange to black, leading to a reddish brown precipitate. The addition process was performed at ambient atmosphere without the protection of inert gases or vacuum atmosphere. Finally, the supernatant was discarded by decantation. The resulting solid products were washed with double distilled water and dried at room temperature naturally.

2.3. Fabrication of γ-Fe_2O_3 nanoribbon and α-Fe_2O_3 nanospheres modified GCE

Prior to modification, the GCE was polished to a mirror-like surface with 1, 0.3 and 0.05 μm alumina slurry and rinsed thoroughly with doubly distilled water between each polishing step. Then, it was washed successively with doubly distilled water in an ultrasonic bath and dried in air. About 1 mg of iron oxide nanoparticles were dispersed in 3 mL ethanol under ultrasonication. The iron oxide modified GCE were obtained by casting 5 μL of these suspensions on the surface of the electrochemically cleaned GCE, which were dried in air at room temperature. The modified GCE was activated in 7.4 Phosphate buffer solution by successive cyclic scans between -0.2 and $+0.8$ V. Before and after each experiment, the modified GC electrode was washed with distilled water and reactivated by the previously mentioned method.

2.4. Characterization

The nanostructure characteristics were studied using a field emission scanning electron microscope (SEM, Hitachi MODEL S-4800). TEM images were obtained from JEOL JEM 2010 transition electron microscope operating at 200 kV. X-ray diffraction Spectroscopy study (XPERT-PRO with Cu Kα radiation (λ = 0.154060 nm) on Panlytical X'Pert Pro Diffractometer) was used for studying the structural phase identification. Fourier transform infrared spectrometer (FT-IR, Nicolet 5700) was performed to analyze the surface characteristics of the nanoparticles. X-ray photoemission spectroscopy was recorded on a Kratos ASIS-HS X-ray photoelectron spectroscope equipped with a standard and monochromatic source (Al Ka) operated at 150 W (15 kV, 10 mA). The magnetization curves and hysteresis loop of the nanostructures were characterized with a Lake model 7300 VSM. Cyclic voltammogram (CV) tests were performed by a CHI6131D Electrochemical Impedance Analyzer (USA) using the as-modified electrode and bare GC electrode as working electrode, a platinum wire was the counter electrode, and saturated calomel electrode (SCE) was the reference electrode. CV curves were examined in the voltage range of -0.2–0.8 V at a scan rate of 50 mV s^{-1}.

3. Results and discussion

To understand the growth process of the products, the morphology evolution of the iron oxide spherical and ribbon like superstructures have been studied by FE-SEM and TEM images. The possible formation processes and the FE-SEM images of the samples obtained with different reaction time and concentration of bio-surfactant are shown in Fig. 1. Three different forms of iron oxides like Fe_3O_4, γ-Fe_2O_3 and α-Fe_2O_3 nanostructures are synthesized without the use of any complex precursors, templates, or

reagents that can induce the directed growth of nanocrystals and the formation of nanoribbon like structures in a single reaction is achieved in one step single pot process. Reaction time is one of the key factors for the growth of the crystal of particular shape. To scrutinize the growth process of the γ-Fe_2O_3 nanoribbons, time dependent evolution of the morphology has been studied at ambient temperature. The FE-SEM observations indicated that, at an earlier stage (Fig. 1a and d) of the co-precipitation reaction in the 2% of bio-surfactant, the product mainly composed of only small Fe_3O_4 iron oxide nanocrystals of 10 nm with monodispersed spherical morphology generated through conventional nucleation and subsequent crystal growth mechanism. As the reaction time is prolonged for 2 hrs, part of the nanospherical particles were begin to combine with each other and the products were totally transformed in to large quantities of γ-Fe_2O_3 nanoribbon shaped morphology (Fig. 1b and e).

We can see that on conversion from Fe_3O_4 to γ-Fe_2O_3, there is a topotactic phase change occurs through imperfect oxidation of Fe_3O_4. During the oxidation process of Fe_3O_4 nanospheres, there is a possibility to form γ-Fe_2O_3 nanospheres on the surface of the Fe_3O_4 spherical nanoparticles. Since the specific volume of the Fe_2O_3 is slightly larger than that of Fe_3O_4, compressive stresses are generated and accumulated at the interface between Fe_3O_4 and Fe_2O_3 because of the volume shrinkage.[20] Under the influence of compressive stress, dipole interactions and the thermodynamic driving force, the neighboring nanodots of γ-Fe_2O_3 have a tendency to join each other through the oriented attachment of initially formed spherical nanodots to share the same crystallographic orientations. Through the outward diffusion of Fe ions along the grain boundaries, iron cations are deposited on to the γ-Fe_2O_3 nanoparticles, where γ-Fe_2O_3

spherical nanoparticles serve as the structural templates for the nucleation of γ-Fe_2O_3 nanoribbons. Together with the subsequent production and deposition of γ-Fe_2O_3 nanoparticles, γ-Fe_2O_3 ribbon-like nanostructures were formed. Moreover, we have also been observed that the reaction time increases after 30 minutes, the color of the solution slowly changes from black (Fe_3O_4) to reddish brown and then the color did not change anymore with reaction time. The characteristic reddish brown color of γ-Fe_2O_3 iron oxide solution offered a convenient visual signature to indicate their formation. Consequently, we kept this reaction time as optimum for all other reactions carried out for various concentrations of bio-surfactant and the structure of greener saponin present in the AV extract is given in the Fig. 2. The above discussion mainly concerns the evolution of the morphology and phase change occurs over the reaction time; more in-depth investigations are still underway to further understand the detailed influences of other factors on the formation, assembly, and the ripening process of the iron oxide crystals.

Furthermore, to understand more about the formation of γ-Fe_2O_3 nanoribbon, the influence of bio-surfactant at various concentrations were also investigated (Fig. 5). At first, the experiments were conducted with a fixed mass of ferric and ferrous ions but various concentrations or quantities of AV extract (bio-surfactant) and a series of iron oxide nanostructures including γ-Fe_2O_3 nanoribbon and α-Fe_2O_3 nanospheres were synthesized. The experiments carried out at lower concentrations (0.5%,1%,2% and 3%) of bio-surfactant, only nanoribbons were formed with low aspect ratio (10). The aspect ratio of the nanoribbon increases (10, 12, 15, and 18) with increasing the concentration of bio-surfactant (Fig. 5a-d). The higher aspect ratio may be due to the increased length and slight increment in diameter of the ribbon. However, the reaction undergoes

morphological changes of nanospherical particles in to nanoribbon formation at 2% concentration for various time intervals. It seems to be caused by the irreversible binding of strongly binding bio-surfactant on the central region of the growing nanoparticles.[21] The whole process includes nucleation, surface regularity, growth and oriented attachment. Initially, the crystal would nucleate from the precursor solution, simultaneously the growth habit of the nanoribbon is emerged. The –OH groups of the saponin molecules present in the bio-surfactant (Fig. 2) would easily attach to the surface of crystal faces and slowed down the growth rate of the crystal at a given crystallographic orientations.[22] After the fusion of two nanospheres, the third nanosphere will be bound on the edge (instead of the central region where bio-surfactant was strongly bound), generating a catenated structure. The continued growth of nanospheres on the edge of the growing nanoparticles would generate unidirectional nanoribbons. Under the capping effect of greener saponin, crystals preferentially grow along the long chain of saponin and finally ribbon like morphology would form via oriented attachment. At this juncture, the bio-surfactant acts as a structure directing agent for the growth of the γ-Fe_2O_3 nanocrystals mainly along the direction (311 plane) by absorbing on the surface of the iron oxide as seen from the XRD (Fig. 3a). Conversely, the higher concentration (10%) of the bio-surfactant strongly competes with the iron oxide nanostructures, does not help in growing the structure of nanoribbon. Only α-Fe_2O_3 nanospherical morphology with an average particle size of 12 nm is formed and the particle distribution is relatively homogeneous (Fig. **1c** and f). At this time, more amount of bio-surfactant may form micelles on the surface of the particles after the nucleation, thereby prohibiting the further growth in such a way. The ability of the micelles to arrest the growth of the particles is to

become stronger in response to the increase in surfactant amount, so the average particle size decreases, finally leading to the homogeneous dispersal of the spherical nanoparticles. Additionally, more surfactant can provide more opportunities to contact with the surface at any direction of the spherical α-Fe$_2$O$_3$ nanoparticles. It also means that the distribution of the surfactant in various direction of the surface of the α-Fe$_2$O$_3$ nanoparticles is highly isotropic, so it can be found that the better size distribution in the process of the crystal growth could be obtained with the more befitting amount of the surfactant used in the reaction.[23] This idiosyncratic property of the saponin rich bio-surfactant not only plays a vital role to design the morphology of Fe$_3$O$_4$ and γ-Fe$_2$O$_3$, but also play a key role in forming α-Fe$_2$O$_3$ phase of iron oxide.

The highly crystalline Fe$_3$O$_4$, γ-Fe$_2$O$_3$ and α-Fe$_2$O$_3$ phase transformation for the obtained iron oxide products have been confirmed with the X-ray diffraction method and the corresponding XRD patterns of the samples are shown in the Fig. 3a. All the reflections can be indexed to a cubic spinel phase of Fe$_3$O$_4$ (Magnetite, JCPDS No. 89-0951), γ-Fe$_2$O$_3$ (Maghemite, JCPDS No. 89-5892) and pure rhombohedral phase of α-Fe$_2$O$_3$ (Hematite, JCPDS No. 33- 0664). The XRD spectra of the spherical nanoparticles formed at 30 min indicate the formation of Fe$_3$O$_4$ phase, but the nanoribbon grown at 2% bio-surfactant in 2 hrs exhibit the pure form of γ-Fe$_2$O$_3$ with cubic spinel structure with a very small intensity peak matching with the Fe$_3$O$_4$ phase in the initial stage of crystal growth. The γ-Fe$_2$O$_3$ nanoribbon grows through the oriented attachment particularly along the <311> direction, which gives rise to relatively intense diffraction peak of the (311) plane. However, the iron oxide samples synthesized from increased bio-surfactant (10%), the samples show pure α-Fe$_2$O$_3$ phase**.** Additionally, the appearance of two

dominant peaks for (110) and (104) planes also confirm the presence of α-Fe_2O_3 phase. Whereas, the bio-surfactant varied from 0.5% to 3%, only pure phase of γ-Fe_2O_3 nanoribbons are formed without any discrepancies (Fig. S1†). The increased intensity of XRD peaks for the Fe_3O_4 and α-Fe_2O_3 spherical nanoparticles are noted compared to the γ-Fe_2O_3 nanoribbon as can be visualized in the FE-SEM images (Fig. 1). At the same time, the intensity of the diffraction peaks is a size dependent behavior, the aspect ratio of the nanoribbon increases with increasing the concentration of bio-surfactant (Fig. S1†) and the diffraction pattern shrinks.[24] However, the XRD patterns of magnetite and maghemite just differ in a few low intensity reflections and very difficult to differentiate them. Further investigations are carried out to examine the Fe_3O_4, γ-Fe_2O_3 and α-Fe_2O_3 phases. First, the colors of our samples are observed and the characteristic black color of Fe_3O_4 which is significantly different from that of γ-Fe_2O_3 (reddish-brown) and α -Fe_2O_3 (red). Secondly, a sensitive XPS measurement have been consulted to unambiguously assigned the crystal phase of Fe^{2+} and Fe^{3+} cations.[25]

In our case, the levels of $Fe2p_{3/2}$ and $Fe2p_{1/2}$ for γ-Fe_2O_3 and α-Fe_2O_3 are appeared at 710.8 and 724.4 eV; 710.5 and 724.2 respectively. However, the levels are emerged at higher binding energy of 711.1 and 724.9 eV for Fe_3O_4 and a satellite peak at around 719.4 and 719.2 eV is observed for γ-Fe_2O_3 nanoribbon and α-Fe_2O_3 nanospheres respectively (Fig. 3b). It is in good agreement with the literature that the peaks shift to high binding energy with broadening for Fe_3O_4 due to the appearance of $Fe^{2+}(2p_{3/2})$ and $Fe^{2+}(2p_{1/2})$. A shoulder around 711 eV seems to appear in Figure 3b, which further evidences that the initially formed spherical nanoparticles are Fe_3O_4 iron oxide.[26,27] In addition, the presence of the satellite peak at 719.4 eV is the characteristic of γ-Fe_2O_3,

while the satellite peak in Fe_3O_4 is covered and becomes less resolved.[28] The XPS patterns are well in agreement with the XRD data and revealed the complete phase transformation of Fe_3O_4 in to γ-Fe_2O_3 and morphological changes could be achieved by carefully controlling the reaction conditions (Fig. 3a and b).

Thermal analysis further supports the iron oxide phase transformation from Fe_3O_4 in to γ-Fe_2O_3. The Fe_3O_4 nanospheres show 27.4% weight loss below 110º C resulting from the removal of adsorbed water which is only 11.3% for the 120 minutes grown γ-Fe_2O_3 nanoribbon. This peculiar interesting behavior may be due to the surface availability (finite size effect) to anchoring the water molecule (-OH) (Fig. 1a and d). A notable weight gain has been observed for Fe_3O_4 nanospherical particles at 200 ºC, which is due to the oxidation behavior of Fe_3O_4 to γ-Fe_2O_3, which is overlapped with the decomposition of the bio-surfactant (Fig. S2†). Above 330 ºC, stable residue could reasonably be ascribed to the pure γ-Fe_2O_3 phase. The result can also be confirmed by the XRD and XPS analysis (Fig. 3a and b). The FT-IR spectra of Fe_3O_4 nanospheres, γ-Fe_2O_3 nanoribbons and α-Fe_2O_3 nanospheres and the different % (0.5%, 1%, 2% 3% and 10%) of bio-surfactant have been illustrated in the Fig. S3a and b†. The intense and broad band appearance in the region 3200 – 3600 cm^{-1} can be noted, where the iron oxide surfaces are readily bound with hydroxyl groups in an aqueous environment. The absorption band appeared below 700 cm^{-1} is attributed to Fe-O stretching vibration, indicates the formation of iron oxide nanostructures.[29]

We know that the iron-based materials often have intriguing magnetic properties influenced by the structure, shape anisotropy, and crystallinity of the nanostructured materials.[30] Therefore, we have examined the magnetic properties of Fe_3O_4 nanosphers,

γ-Fe_2O_3 nanoribbon and α-Fe_2O_3 spherical nanoparticles and are presented in the Fig. 4. The room-temperature hysteresis curves for a series of samples show neither remanence nor co-ercivity, regardless of the nanocrystal size and shape, and therefore indicate a superparamagnetic behavior. The saturation magnetization (Ms) of Fe_3O_4 nanospheres, γ-Fe_2O_3 nanoribbon and α-Fe_2O_3 spherical nanoparticles is 40, 31 and 1.06 emu/g, the decrease in Ms value of the iron oxide nanoparticles compared to bulk materials is most likely attributed to the decrease in particle size,[31-34] the spin disorder on the surface and surface oxidation would significantly reduce the total magnetic moment. From this fact, here also the Fe_3O_4 spherical nanoparticles formed at 30 min undergoes oxidation and forms γ-Fe_2O_3 nanoribbons at 120 min in 2% bio-surfactant. The observed magnetic property of α -Fe_2O_3 spherical nanoparticles synthesized at 10% bio-surfactant is a result of the high surface to-volume ratio (S/V) of the formed nanostructures.[35] Compared to nanoribbon, α-Fe_2O_3 nanospheres have much higher S/V, therefore the high percentage of surface atoms was linked to the bio-surfactant and the surface effects generate a magnetic dead layer on the particle surface. Further support to this interpretation is provided by the recognition of a clear paramagnetic component (i.e., linear dependence of Ms vs H) which prevents the hysteresis curves from becoming flat at saturation, especially in the sample with the lowest Ms value. We have also been explored the magnetic properties of iron oxide nanostructures synthesized at various concentration (0.5% to 10%) of bio-surfactant (Fig. S4†). Interestingly, in γ-Fe_2O_3 nanoribbons, the MS drops become even more pronounced as the length of the ribbon increases and/or their diameter narrows. Therefore, more anisotropically the ribbons grow, the more MS is depressed, despite of the actual increase in the nanocrystal volume. Such results clearly indicate that the

magnetic states of the nanocrystals evolve gradually as a function of both the particle's size and shape.

The electrocatalytic oxidation of DA and UA on γ-Fe_2O_3 nanoribbon and α-Fe_2O_3 nanospheres modified GCE in 7.4 PBS in the potential range of -0.2 to +0.8 V at 50 mVs^{-1} scan rate have been carried out using Cyclic voltammetry. Fig. 6 and 7 show the voltammetric responses of the DA and UA at bare GCE and γ-Fe_2O_3 nanoribbon and α-Fe_2O_3 nanospheres modified GCE respectively. The iron oxide nanostructures modified GCE reduces the anodic over potentials of DA & UA and exhibits well-defined anodic peaks compared with the bare GCE. At the bare GCE, UA shows an oxidation peak at 0.52 V. It is well known that the oxidation of UA at the bare GC electrode is generally believed to be totally irreversible and requires high over potential. However, the UA voltammogram obtained on γ-Fe_2O_3 nanoribbon and α-Fe_2O_3 nanospheres modified GC electrode showed an oxidation wave at 0.33 V and 0.37 V potential range respectively with increased current response (100% for γ-Fe_2O_3 nanoribbon) (Fig. 6). DA demonstrates an oxidation peak at 0.30 V at the bare GCE. Conversely, the DA voltammogram obtained on γ-Fe_2O_3 nanoribbon and α-Fe_2O_3 nanospheres modified GC electrode showed an oxidation wave at a reduced potential 0.13 and 0.22 V respectively (Fig. 7) with the enhanced peak current, are attributed to the excellent adsorption ability of γ-Fe_2O_3 nanoribbon and α-Fe_2O_3 nanospheres.

The above results demonstrate that the iron oxide nanostructures modified GC electrode not only accelerate the oxidation of DA and UA, and also significantly enlarged the peak separation among DA and UA. The enlarged anodic peak potential separation coupled with the increased sensitivity renders simultaneous determination of DA and UA

feasibly. Here, the γ-Fe$_2$O$_3$ nanoribbon and α-Fe$_2$O$_3$ nanospheres modified GCE exhibits

well-defined two separate anodic peaks for the oxidation of DA and UA simultaneously

with the enhanced current response using CV (Fig. 8). The presence of functional groups

on iron oxide nanostructures modified GCE resolved the mixed voltammetric response of

these species (DA and UA) into two well-defined voltammetric peaks at the potentials of

0.19 and 0.48 V (0.29 V peak separation) for γ-Fe$_2$O$_3$ nanoribbon and 0.23 and 0.50 mV

(0.27 V peak separation) for α-Fe$_2$O$_3$ nanospheres modified GCE respectively. Further

the peak separation between the DA and UA on γ-Fe$_2$O$_3$ nanoribbon and α-Fe$_2$O$_3$

nanospheres is sufficiently enough to oxidize them as a well-defined two separate peaks

for the easy determination, where γ-Fe$_2$O$_3$ nanoribbon modified GCE is best as it exhibits

0.29 V wide separations between DA and UA voltammetric response with increased peak

current. The reason for this improved catalytic activity of γ-Fe$_2$O$_3$ nanoribbon is the 1D

nanostructure acts as an electron wire, where the electron diffusion takes place at faster

rate. The α-Fe$_2$O$_3$ nanospheres also exhibit better performance than that of flat electrode

(bare GCE). The inferiority of the α-Fe$_2$O$_3$ nanospheres compared to γ-Fe$_2$O$_3$ nanoribbon

is due to the increased intercontacts among the distributed ions. The outcome of the

voltammetric responses indicate that the electrocatalytic reaction on the iron oxide

nanostructures facilitates the electron transfer between electrode and the analyte

molecules, as a result the electrochemical oxidation of DA and UA becomes easier. The

iron oxide nanostructures can act as a promoter to increase the rate of electron transfer,

lowers the over potential of DA and UA modified electrode, it is clear that the iron oxide

nanostructures modified GC electrodes can be successfully used for the determination of

biomolecules and bioelectronics/biosensor applications.

4. Conclusions

In summary, a facile environmentally benign shape controlled synthesis of anisotropic crystalline iron oxide nanostructures using saponin rich Aloevera extract as a bio-surfactant and shape directing agent has been explored. By carefully monitoring the reaction parameters, the aspect ratio of the γ-Fe$_2$O$_3$ nanoribbon and morphology of the nanostructures could be designed. The saponin molecules present in the AV extract played a key role in the formation of γ-Fe$_2$O$_3$ nanoribbon and it was a kinetically controlled process. The obtained γ-Fe$_2$O$_3$ nanoribbon and α-Fe$_2$O$_3$ nanospheres exhibited a high electrocatalytic activity towards the oxidation of DA and UA by significantly decreasing their oxidation over potentials with the enhanced peak currents. Large peak separation between DA and UA could be obtained, indicating that the modified GCE facilitated their simultaneous determination. With excellent selectivity and high sensitivity, 1D γ-Fe$_2$O$_3$ nanoribbon showed better electrochemical response towards DA and UA than the α-Fe$_2$O$_3$ nanospheres. The present simple synthetic greener method provides high-yield nanosized materials with good magnetic properties, and this method can be used to prepare nanocrystalline oxides of other interesting materials. Therefore, we strongly believe that the use of saponin rich bio-surfactant offer a large scale production of biocompatible iron oxide nanostructures that can be used as a vehicle for biomedical/sensing applications. However, the role of AV extract is not yet specified and the complexation between bio-surfactant and iron ions in the solution is still unknown, and it is under investigation.

Acknowledgements

The authors wish to thank the Department of Physics, Alagappa University, Karaikudi, India for providing XRD analysis and National Taipei University of Technology, Taiwan for providing TEM facility.

References

1   P.M. Rao and X. Zheng, *Nano Lett.,* 2011, **11**, 2390–2395.

2   D.H. Reich, M. Tanase, A. Hultgren, L.A. Bauer, C.S. Chen and G.J. Meyer, *J. Appl. Phys.,* 2003, **93**, 7275–7280.

3   X. Xu and M.B. Cortie, *J. Phys. Chem. C,* 2007, **111**, 18135–18142.

4   J. Dobson, *Drug DeV. Res.,* 2006, **67**, 55–60.

5   W. Wu, Q.G. He and C.Z. Jiang, *Nanoscale Res. Lett.,* 2008, **3**, 397–415.

6   M. Shokouhimehr, Y.Z. Piao, J. Kim, Y.J. Jang and T. Hyeon, *Angew. Chem., Int. Ed.* 2007, **46**, 7039–7043.

7   Y.G. Sun and Y.N. Xia, *Science*, 2002, **298**, 2176-2179.

8   V.F. Puntes, K.M. Krishnan and A.P. Alivisatos, *Science*, 2001, **291**, 2115-2117.

9   C. Burda, X. Chen, R. Narayanan and M.A.E. Sayed, *Chem. ReV.,* 2005, **105**, 1025-1102.

10   M.C. Daniel and D. Astruc, *Chem. ReV*., *2004*, **104**, 293-346.

11   H. Itoh and T.J. Sugimoto, *Colloid Interface Sci.,* 2003, **265**, 283–295.

12   Y. Piao, J. Kim, H.B. Na, D. Kim, J.S. Baek, M.K. Ko, J.H. Lee, M. Shokouhimehr and T. Hyeon, T. Nat. Mater. 2008, 7, 242–247.

13   Z. Peng, M. Wu, Y. Xiong, J. Wang and Q. Chen, *Chem. Lett.,* 2005, **34**, 636–637.

14   G. Wang, G. Whittaker, A. Harrison and L. Song, *Mater. Res. Bull.,* 1998, **33**, 1571–1579.

15   R.V. Kumar, Y. Koltypin, X.N. Xu, Y. Yeshurun, A. Gedanken, I. Felner, *J. Appl. Phys.,* 2001, **89**, 6324–6328.

16   Z. Liu, D. Zhang, S. Han, C. Li, B. Lei, W. Lu, J. Fang and C. Zhou, *J. Am. Chem. Soc.,* 2005, **127**, 6–7.

17   S. Laurent, D. Forge, M. Port, A. Roch, C. Robic, L. Vander Elst and R. N. Muller, *Chem. Rev.* 2008, **108***, 2064–2110.

18   D.E. Zhang, X.J. Zhang, X.M. Ni, H.G. Zheng and D.D. Yang, *J. Magn. Magn. Mater.,* 2005, **294**, 10–15.

19   A. Bharde, D. Rautaray, V. Bansal, A. Ahmad, I. Sarkar, S.M. Yusuf, M. Sanyal and M. Sastry, *Small*, 2006, **2**,135 – 141

20   R. S. Cai, T. Li, Y. Q. Wang, C. Wang, L. Yuan and G. W. Zhou, *J Nanopart Res*,2012, **14**, 1073-1083.

21   S.J Park, S. Kim, S. Lee, Z.G. Khim, K. Char and T. Hyeon, *J. Am. Chem. Soc*., 2000, **122**, 8581-8582.

22   Y.Y. Li, J.P. Liu, X.T. Huang and C.Y. Li, *Cryst. Growth Des*.,2007, **7**, 11350–11355.

23   H. Yan, J. Zhang, C. You, Z. Song, B. Yu and Y. Shen, *Mater. Chem. Phys*.,2009, **113**, 46–52.

24   H. Wiogo, M. Lim, P. Munroe and R. Amal, *Cryst. Growth Des.,* 2011, **11**, 1689–1696.

25   S. Palchoudhury, Y. Xu, A. Rushdi, R.A. Hollerb and Yuping Bao, *Chem. Commun*., 2012, **48**, 10499–10501.

26   X. Teng, D. Black, N. Watkins, Y. Gao and H. Yang, *Nano Lett*., 2003, **3**, 261-264.

27   C.R. Brundle, T.J. Chuang and K. Wandelt, *Surf. Sci*., 1977, **68**, 459-468.

28   D. Zhang, Z. Liu, S. Han, C. Li, B. Lei, M.P. Stewart, J.M. Tour and C. Zhou, *Nano Lett*., 2004, **4**, 2151-2155.

29   L. Bao, H. Yang, X. Wang, F. Zhang, R. Shi, B. Liu, L. Wang and H. Zhao, *J.Cryst. Growth*., 2011, **328**, 62–69.

30   G. Sun, B. Dong, M. Cao, B. Wei and C. Hu, *Chem. Mater.,* 2011, **23**, 1587–1593.

31   J. Park, K. An, Y. Hwang, J.G. Park, H.J. Noh, J.Y. Kim, J.H. Park, N.M. Hwang and T. Hyeon, *Nat. Mater.,* 2004, **3**, 891-895.

32   M. Ramalakshmi, P. Shakkthivel, M. Sundrarajan and S.M. Chen, *Mater. Res. Bull.*, 2013, **48**, 2758–2765.

33   F. Mou, J. Guan, H. Ma, L. Xu and Weidong Shi, *Appl. Mater. Interfaces*., 2012, **4**, 3987−3993.

34   N. Pinna, S. Grancharov, P. Beato, P. Bonville, N. Antonietti and M. Niederberger*, Chem. Mater*., 2005, **17**, 3044-3049.

35   P. D. Cozzoli, E. Snoeck, M. A. Garcia, C. Giannini, A. Guagliardi, A. Cervellino, □F. Gozzo, A. Hernando, K. Achterhold, N. Ciobanu, F. G. Parak, R. Cingolani and Liberato Manna, *Nano Lett*., 2006, **6**, 1966-1972.
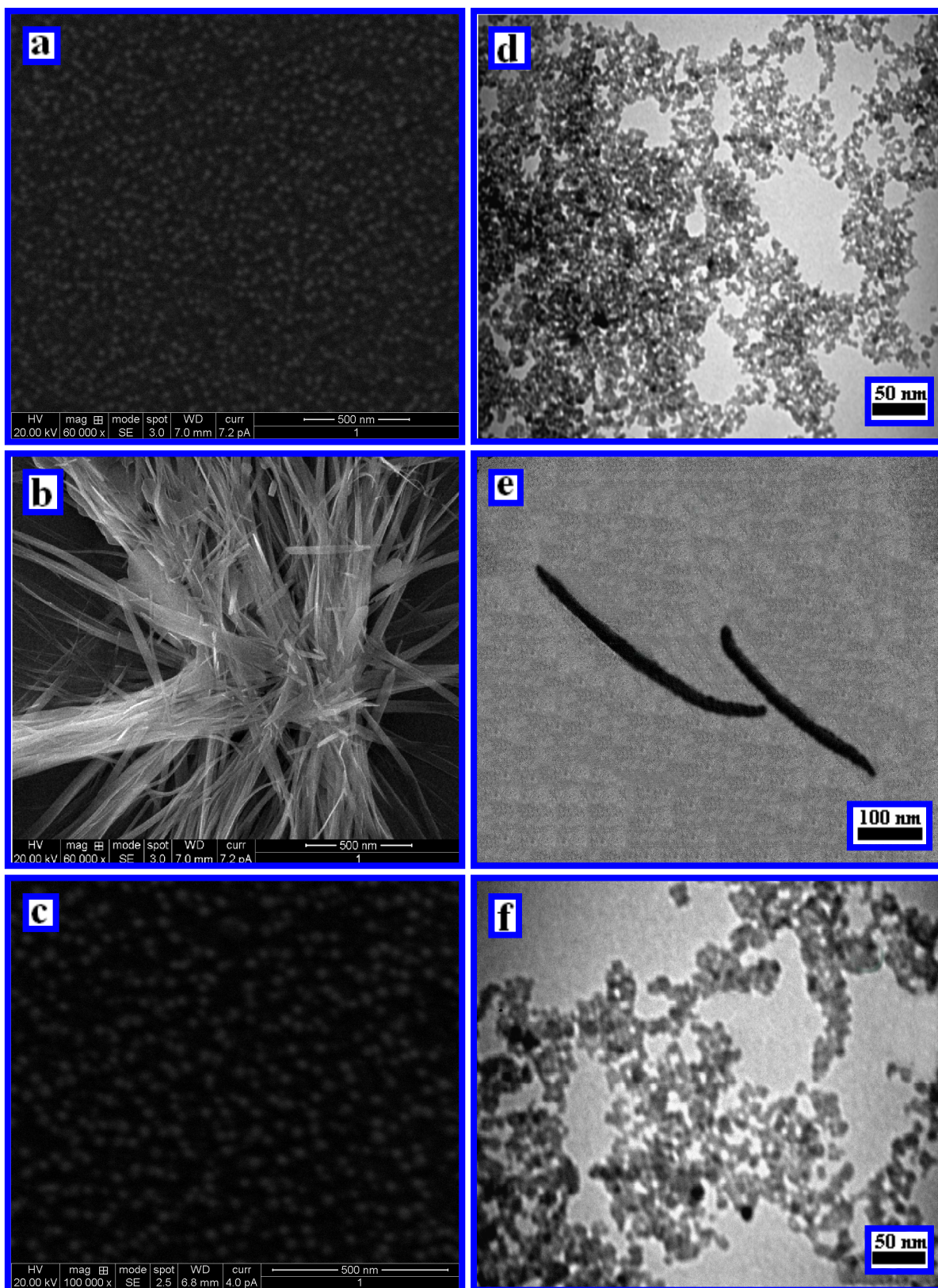
Figure captions

Fig. 1 Iron oxide nanostructures synthesized at various concentration of bio-surfactant for different time intervals at 30 ºC (a) FE-SEM images of 2% Fe_3O_4 nanospheres in 30 mins (b) 2% γ-Fe_2O_3 nanoribbon in 2hrs (c) 10% α-Fe_2O_3 nanospheres in 2hrs (d) TEM images of 2% Fe_3O_4 nanospheres in 30 mins (e) 2% γ-Fe_2O_3 nanoribbon in 2hrs (f) 10% α-Fe_2O_3 nanospheres in 2hrs
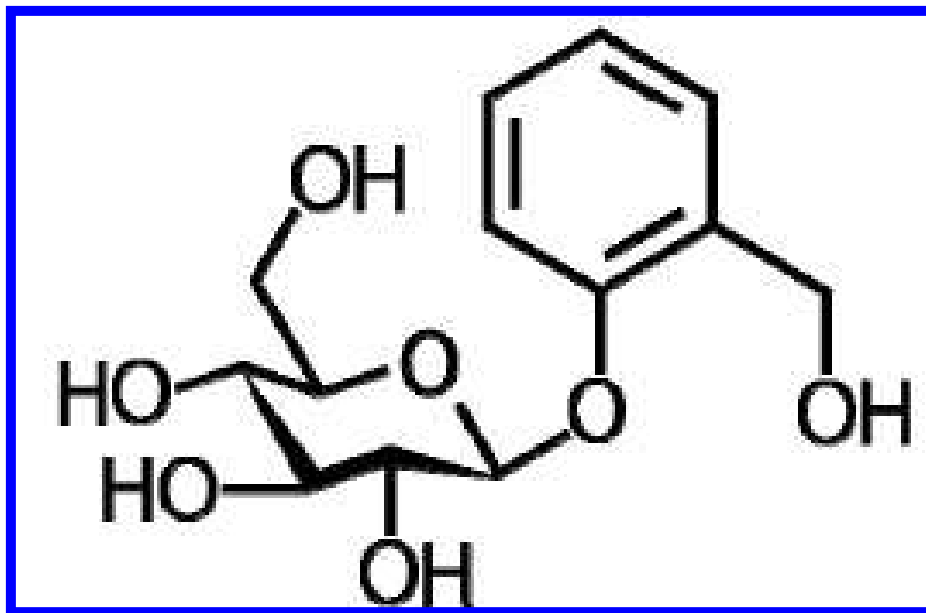
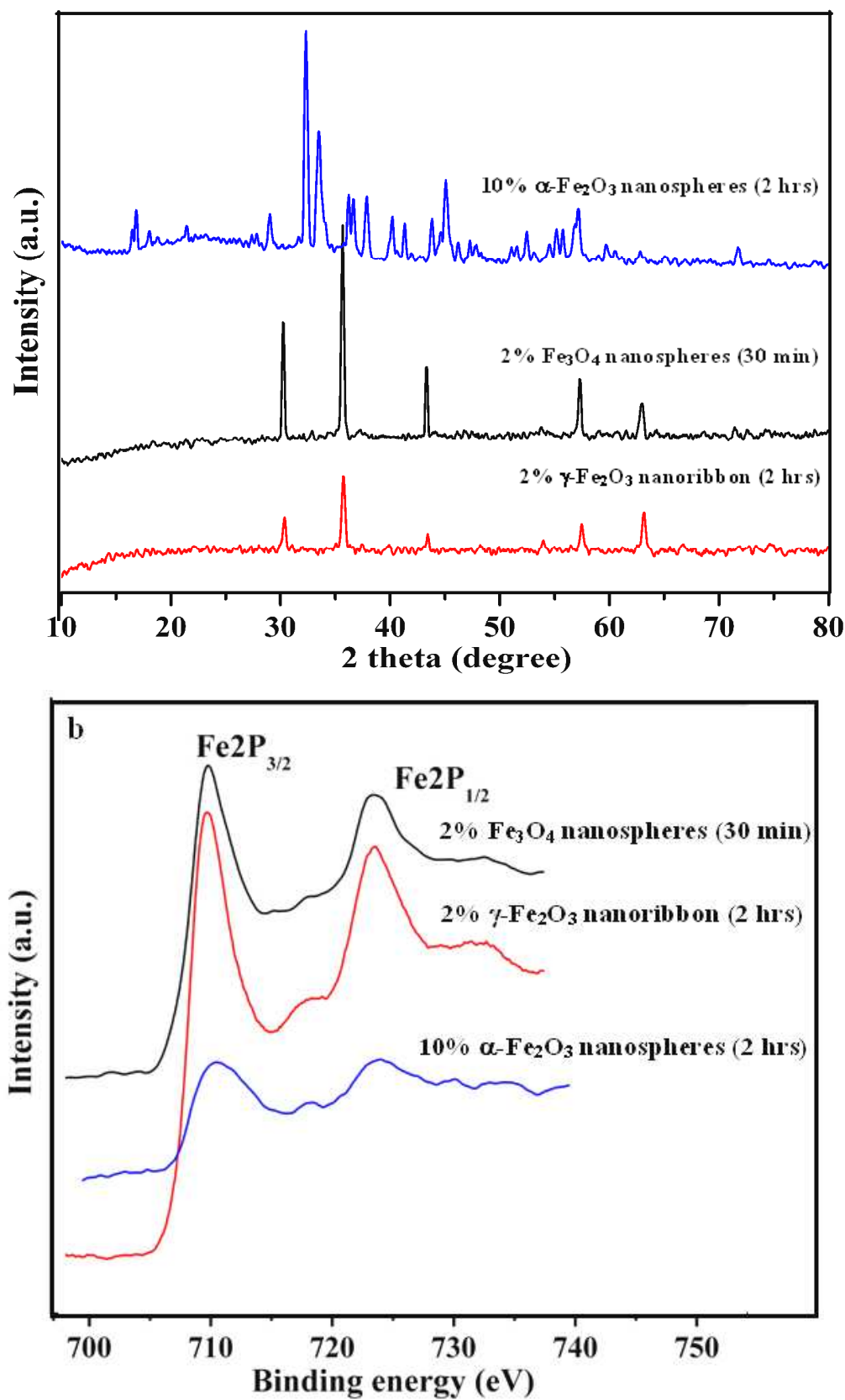**Fig. 2** Chemical structure of Greener Saponin present in the AV extract

Fig. 3 Iron oxide nanostructures synthesized at various concentration of bio-surfactant for different time intervals at 30 ºC. (a) XRD patterns of different polymorphs of iron oxide (b) XPS spectrum of different polymorphs of iron oxide.
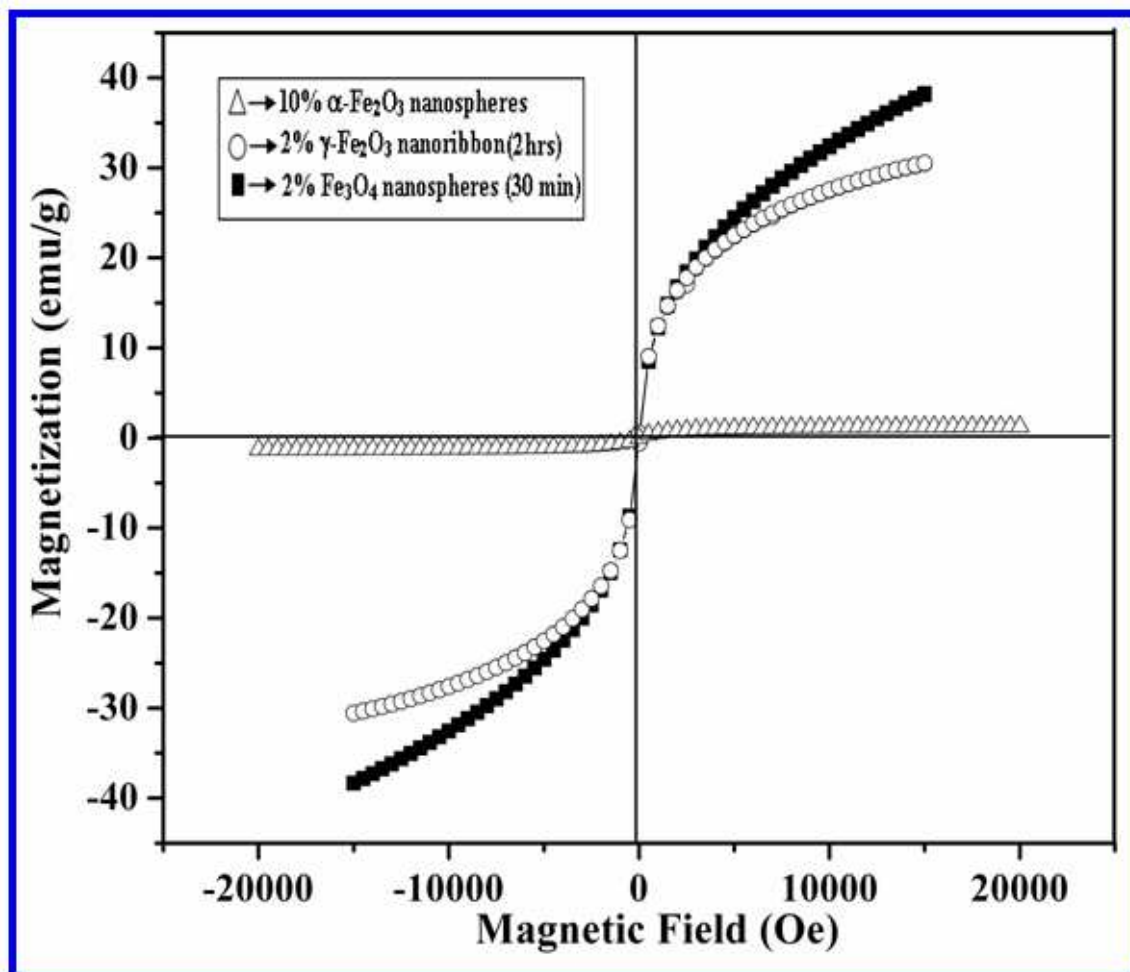
Fig. 4 Magnetization curves of different polymorphs of iron oxide nanostructures synthesized at various concentration of bio-surfactant for different time intervals at 30 ºC.

Fig. 5 FE-SEM images of Iron oxide nanostructures synthesized at various concentration of bio-surfactant at 30 ºC in 2hrs (a) 0.5% nanoribbon (b) 1% nanoribbon (c) 2% nanoribbon (d) 3% nanoribbon (e) 10% nanospheres.

Fig. 6 Cyclic voltammetric response of 0.5 X 10^{-3}M Dopamine in 7.4 PBS at 50 mVs^{-1} (a) bare GCE (b) α-Fe_2O_3 nanospheres and (c) γ-Fe_2O_3 nanoribbon modified GCE.

Fig. 7 Cyclic voltammetric response of 0.5 X 10^{-3}M Uric acid in 7.4 PBS at 50 mVs^{-1} (a) bare GCE (b) α-Fe_2O_3 nanospheres and (c) γ-Fe_2O_3 nanoribbon modified GCE.

Fig. 8 CVs of Simultaneous determination of DA and UA using (a) bare (b) α-Fe_2O_3 nanorspheres (c) γ-Fe_2O_3 nanoribbon modified GCE in 0.5 X 10^{-3}M in 7.4 PBS at 50 mVs^{-1}.

Figures

Fig. 1 Iron oxide nanostructures synthesized at various concentration of bio-surfactant for different time intervals at 30 ºC (a) FE-SEM images of 2% Fe_3O_4 nanospheres in 30 mins (b) 2% γ-Fe_2O_3 nanoribbon in 2hrs (c) 10% α-Fe_2O_3 nanospheres in 2hrs (d) TEM images of 2% Fe_3O_4 nanospheres in 30 mins (e) 2% γ-Fe_2O_3 nanoribbon in 2hrs (f) 10% α-Fe_2O_3 nanospheres in 2hrs

Fig. 2 Chemical structure of Greener Saponin present in the AV extract

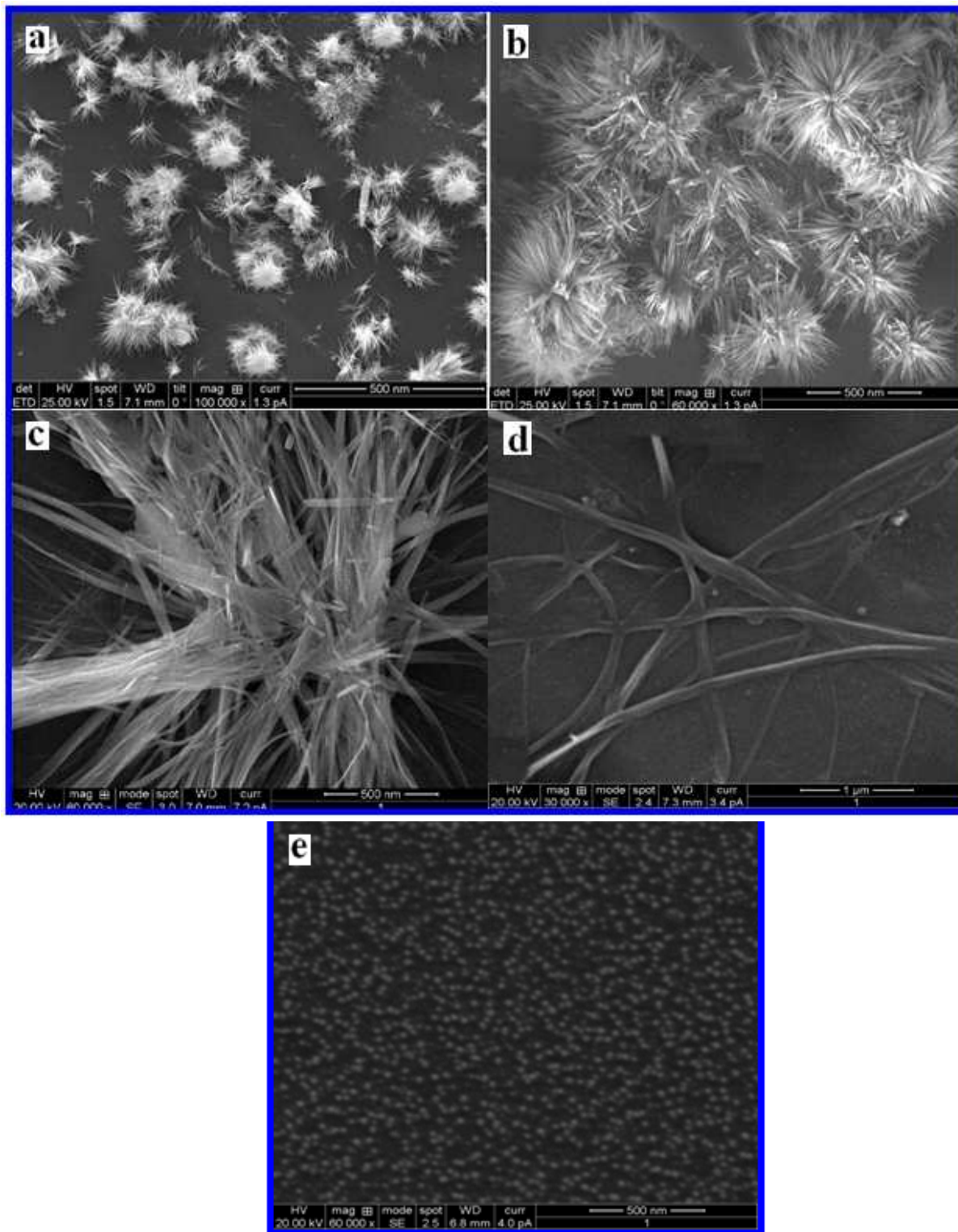**Fig. 3** Iron oxide nanostructures synthesized at various concentration of bio-surfactant for different time intervals at 30 ºC. (a) XRD patterns of different polymorphs of iron oxide (b) XPS spectrum of different polymorphs of iron oxide.

3

Fig. 4 Magnetization curves of different polymorphs of iron oxide nanostructures synthesized at various concentration of bio-surfactant for different time intervals at 30 ºC.

Fig. 5 FE-SEM images of Iron oxide nanostructures synthesized at various concentration of bio-surfactant at 30 ºC in 2hrs (a) 0.5% nanoribbon (b) 1% nanoribbon (c) 2% nanoribbon (d) 3% nanoribbon (e) 10% nanospheres.
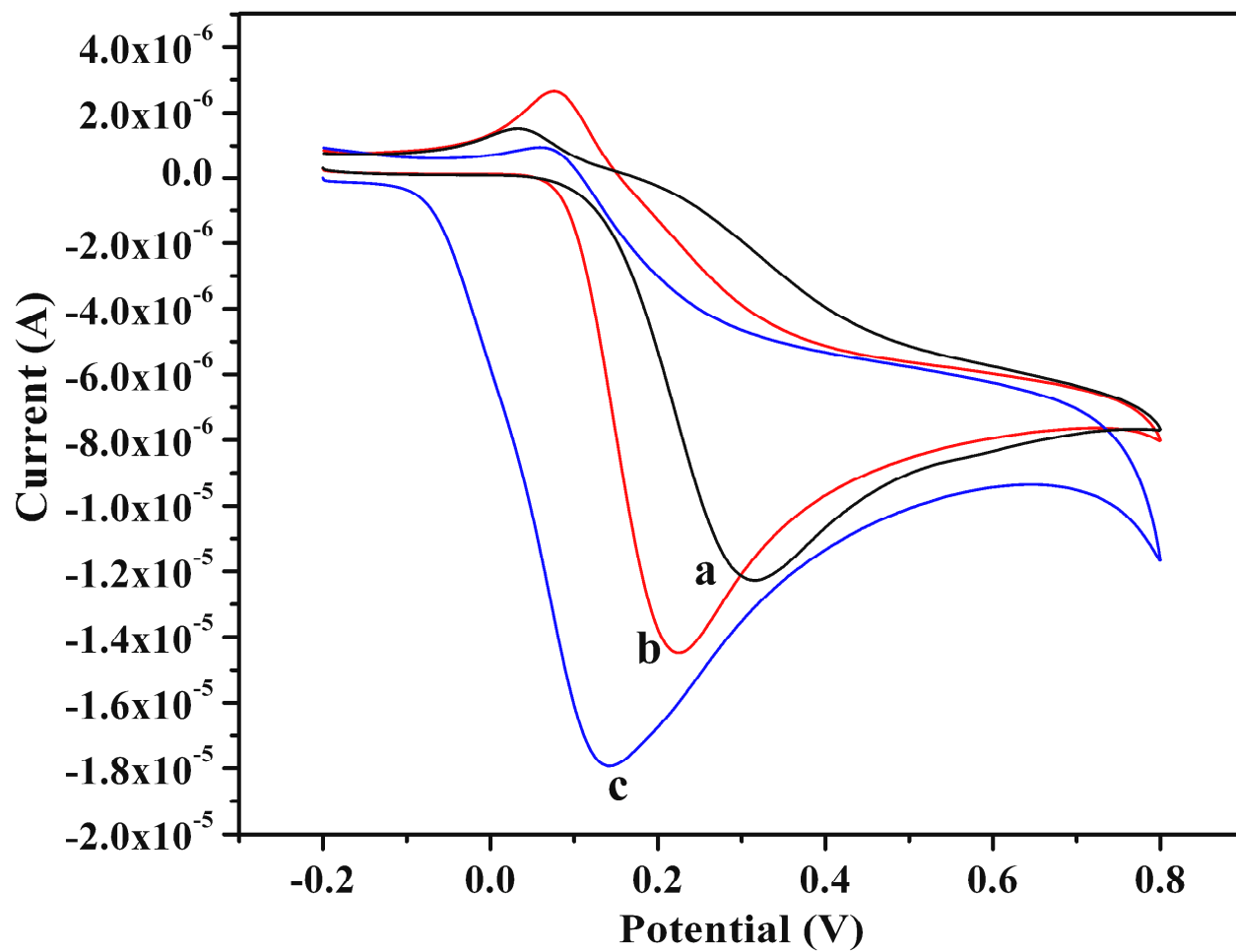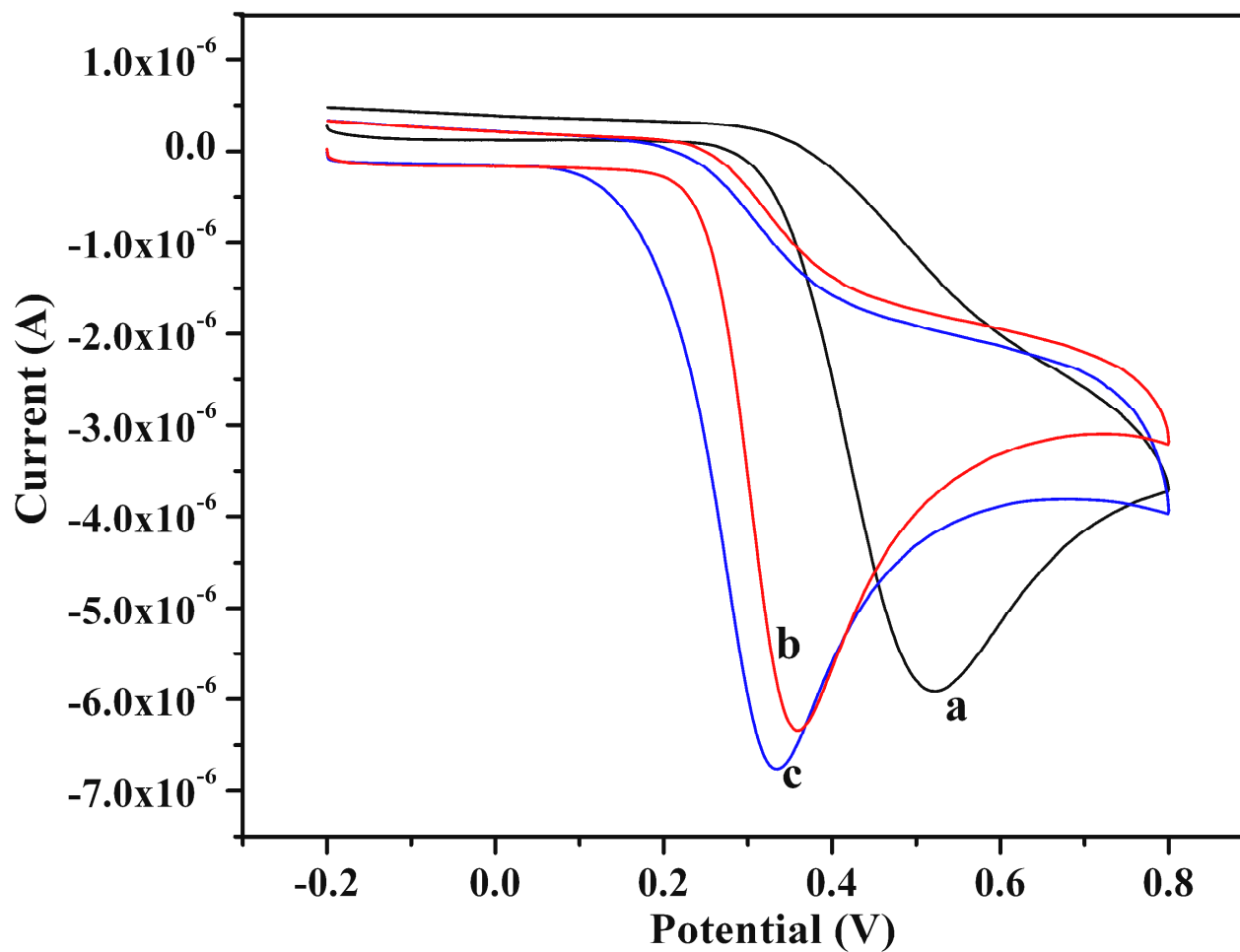
5

Fig. 6 Cyclic voltammetric response of 0.5 X 10^{-3}M Dopamine in 7.4 PBS at 50 mVs^{-1}
(a) bare GCE (b) α-Fe$_2$O$_3$ nanospheres and (c) γ-Fe$_2$O$_3$ nanoribbon modified GCE.

Fig. 7 Cyclic voltammetric response of 0.5 X 10^{-3}M Uric acid in 7.4 PBS at 50 mVs^{-1} (a) bare GCE (b) α-Fe$_2$O$_3$ nanospheres and (c) γ-Fe$_2$O$_3$ nanoribbon modified GCE.
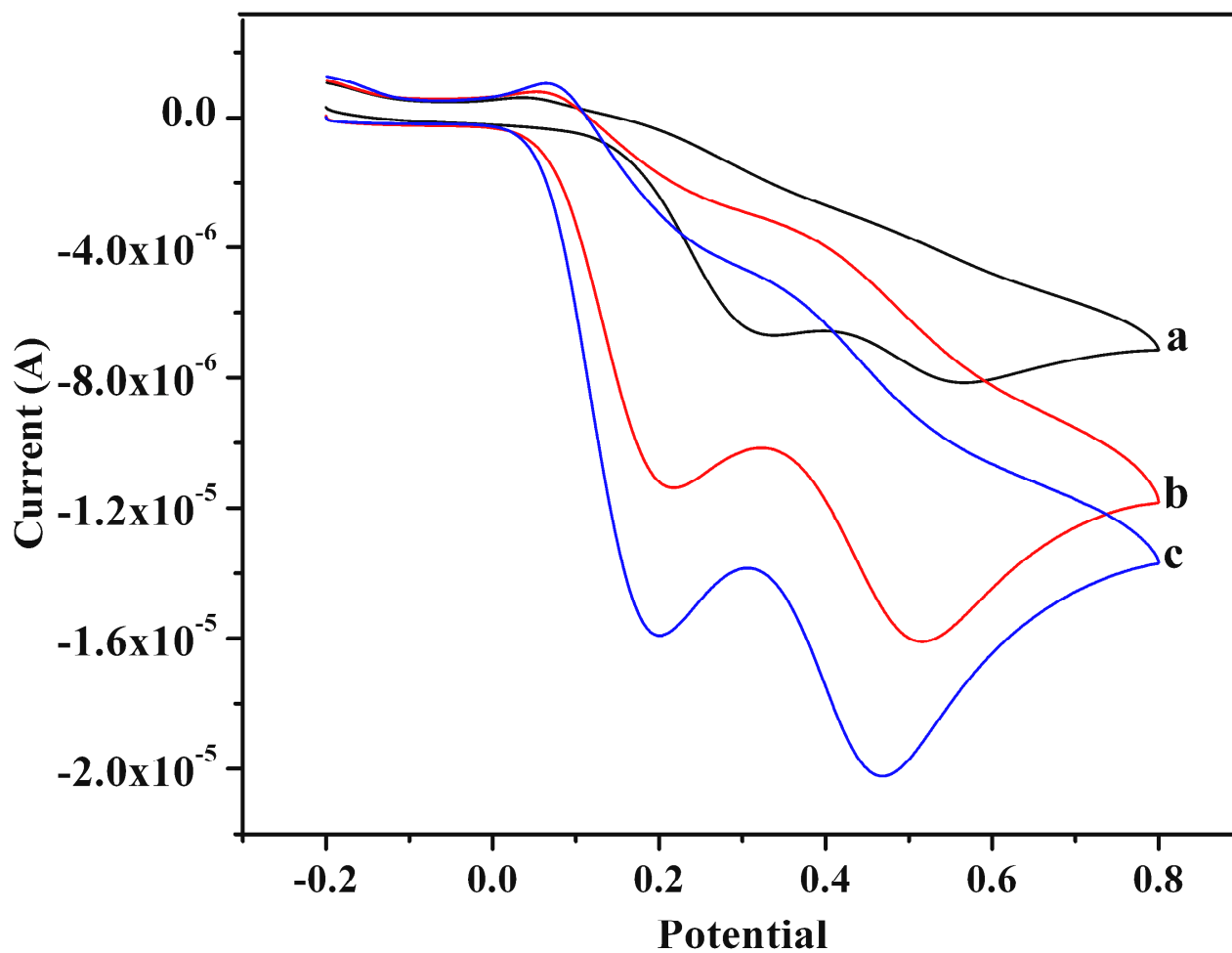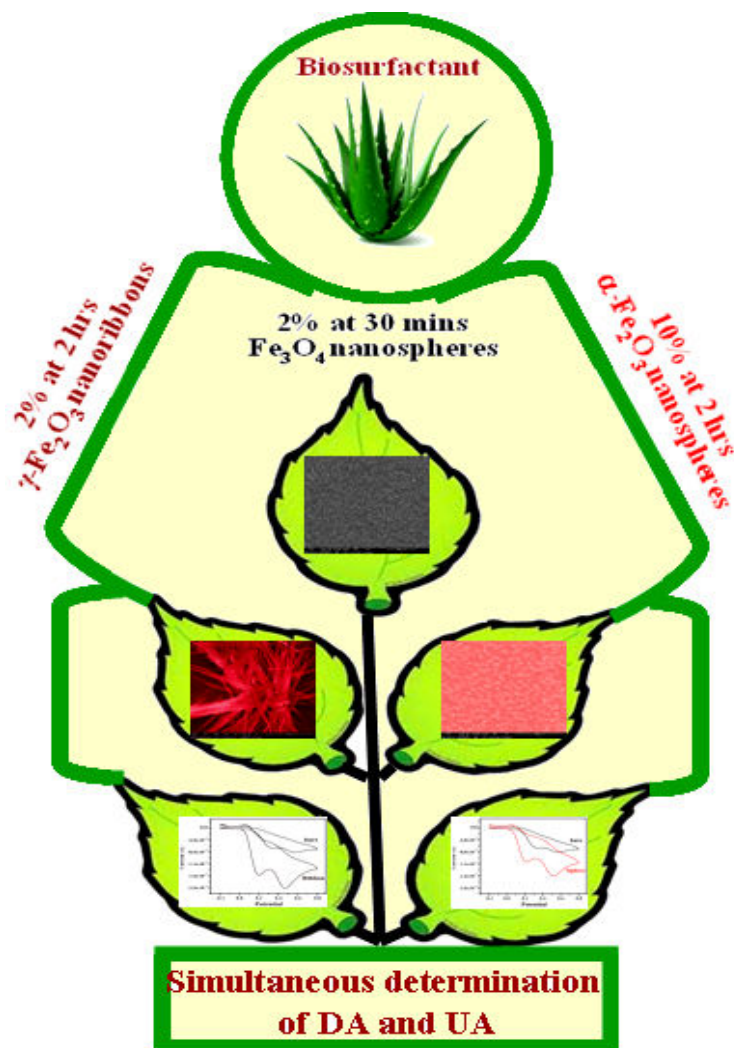
7

Fig. 8 CVs of Simultaneous determination of DA and UA using (a) bare (b) α-Fe_2O_3 nanorspheres (c) γ-Fe_2O_3 nanoribbon modified GCE in 0.5 X 10^{-3}M in 7.4 PBS at 50 mVs^{-1}.

Greener Saponin Induced Morphologically Controlled Various Polymorphs of Nanostructured Iron oxide Materials for Biosensor Applications

Sasikala Sundar and Shakkthivel Piraman*

Biological synthesis of three different polymorphs of iron oxide nanostructures in one-pot reaction through greener saponin have been fabricated for biomolecules determination.